Environmental Science & Technology

pubs.acs.org/est

Article

Quantification of Atmospheric Mercury Deposition to and Legacy Re-emission from a Subtropical Forest Floor by Mercury Isotopes

Wei Yuan, Xun Wang, Che-Jen Lin, Jonas Olof Sommar, Bo Wang, Zhiyun Lu, and Xinbin Feng*

Cite This: https://doi.org/10.1021/acs.est.1c02744

Read Online

ABSTRACT: Air−soil exchange of elemental mercury vapor (Hg^0) is an important component in the budget of the global mercury cycle. However, its mechanistic detail is poorly understood. In this study, stable Hg isotopes in air, soil, and pore gases are characterized in a subtropical evergreen forest to understand the mechanical features of the air−soil Hg^0 exchange. Strong Hg^{II} reduction in soil releases Hg^0 to pore gas during spring−autumn but diminishes in winter, limiting the evasion in cold seasons. $\Delta^{199}Hg$ in air modified by the Hg^0 efflux during flux chamber measurement exhibit seasonality, from −0.33 ± 0.05‰ in summer to −0.08 ± 0.05‰ in winter. The observed seasonal variation is caused by a strong pore-gas driven soil efflux caused by photoreduction in summer, which weakens significantly in winter. The annual Hg^0 gross deposition is 42 ± 33 $\mu g\ m^{-2}\ yr^{-1}$, and the corresponding Hg^0 evasion from the forest floor is 50 ± 41 $\mu g\ m^{-2}\ yr^{-1}$. The results of this study, although still with uncertainty, offer new insights into the complexity of the air-surface exchange of Hg^0 over the forest land for model implementation in future global assessments.

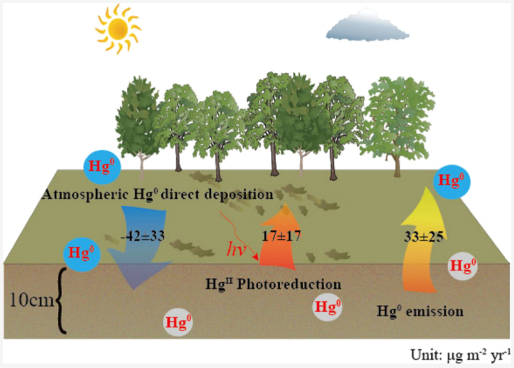

KEYWORDS: *mercury isotope, air−soil exchange, soil pore gas, subtropical forest, mass balance model*

1. INTRODUCTION

As a global persistent pollutant, mercury (Hg) contributes to ecological and health concerns in a variety of ecosystems. The pool of gaseous elemental mercury (Hg^0), the dominant form of Hg in the atmosphere amounts to 5000−5600 Mg.[1,2] About 60% is collectively inherited from natural and legacy emissions, but the knowledge is limited concerning the individual contribution from many of the various types of surfaces in the environment.[2,3] Currently, exchange with forest ecosystems including foliage, bryophytes, soil vegetation, and so forth is the single most uncertain type of Hg^0 flux in magnitude (~±700 Mg yr^{-1}) of all land ecosystems.[3] In general, detailed long-term studies are more unusual, as are those concerning studies of the interaction of Hg^0 with forest floor and soil.[4]

Air−soil Hg^0 exchange in forest ecosystems is a dynamic bi-directional process, including atmospheric Hg^0 gross deposition and Hg^0 evasion,[5−7] and the soil pore Hg^0 gas plays a dominant role in linking the atmospheric Hg^0 to soil Hg^{II} pool.[8−10] The atmospheric gross deposition refers to the process that Hg^0 vapor is passively absorbed or actively retained through oxidative complexation on the forest floor from ambient air. Separating the contribution of gross atmospheric Hg^0 deposition from other processes that makes up Hg^0 fluxes represents a challenge because of the limitation of methodology in determining the individual exchange components.[11] Litterfall deposition has been considered the single largest component in dry deposition in forest ecosystems, causing great gaps with ecosystem-air Hg^0 flux using the meteorology method.[12] Existing data obtained from the dynamic flux chamber method does not account for the total atmospheric gross Hg^0 deposition due to its limited footprint and the isolation of soil from a typical atmospheric environment.[13,14] This leads to uncertainties in estimating the atmospheric Hg^0 dry deposition for global assessments. Microbial reduction, photoreduction, and abiotic dark reduction are considered as the primary pathways that contribute to the pool of Hg^0 in the topsoil layer and indirectly maintain Hg^0 effluxes to the surface air.[15−18] However, no attempt has been made to determine the contribution of each process to fluxes measured by a dynamic flux chamber (DFC) over forest soil.[11]

Data of stable Hg isotope compositions during exchange processes and reservoirs provide insight into the complex exchange processes through the signatures of mass-dependent (MDF) and mass-independent (MIF) fractionation.[19] In addition to the physical, chemical, and biological processes that induce MDF (reported as $\delta^{202}Hg$), Hg MIF signatures,

Received: April 27, 2021
Revised: August 11, 2021
Accepted: August 13, 2021

reported as Δ^{199}Hg and Δ^{201}Hg for odd-MIF and Δ^{200}Hg for even-MIF, may specifically trace reactions and determine the contribution of distinct endmembers. For example, in forest ecosystems, Hg^{II} in precipitation shows predominantly positive odd-MIF and even-MIF and negative values in MDF.[19−21] Soil and forest biomasses display primarily negative odd-MIF and MDF, and insignificant even-MIF,[15,18,21−24] while atmospheric Hg^0 vapor shows negative odd-MIF, positive MDF, and slightly negative even-MIF (only around −0.05‰ in remote sites).[19,23−27] Given the anthropogenic emissions and biomass burning, the atmosphere in Southeast Asia showed the slightly more positive in odd-MIF[28,29] (Δ^{199}Hg = −0.13 ± 0.08‰ and Δ^{201}Hg = −0.12 ± 0.08‰[23−25]) and comparable even-MIF (Δ^{200}Hg = −0.04 ± 0.04‰) compared to other remote sites (Δ^{199}Hg = −0.20 ± 0.08‰, Δ^{201}Hg = −0.17 ± 0.10‰ and Δ^{200}Hg = −0.06 ± 0.04‰[19,25−27,30]). Furthermore, most physico-chemical processes preferentially remove lighter Hg isotopes and result in the heavier isotopes remaining in the residual.[17,31,32] While microbial reduction does not significantly affect odd-MIF,[33,34] abiotic oxidation by natural organic matter (NOM) in the dark gives a positive shift in odd-MIF of the residual pool of Hg^0.[35,36] Moreover, abiotic dark reduction and organosulfur-mediated photoreduction produce a positive odd-MIF shift in the product Hg^0, albeit the MIF is induced through different mechanisms,[37,38] whereas the organic matter-mediated photoreduction driven preferentially by O-donor groups cause a negative odd-MIF shift in the product Hg^0.[39,40]

The objective of the study is to examine the gas exchange of Hg^0 between air and soil isotopically upon exposure to ambient air as well as Hg-free air to estimate the individual contribution of deposition and re-emission of Hg^0 from the forest floor. We systematically observed the seasonal variations of isotopic signatures of Hg^0 in soil pore gas, ambient air Hg^0, and Hg^0 in near-surface air modified by the gas exchange with soil (using a DFC exposed to ambient and Hg-free air) in a subtropical evergreen broadleaf forest ecosystem. Based on the multi-compartmental measurements of Hg isotopic fractionation, we examine the underlying transport and transformations using a stable isotope mass balance model. Finally, the implications of the results for the mercury cycle in forest ecosystems are discussed.

2. METHODOLOGY

2.1. Site Description. The study site is located in the experimental area of the Ailaoshan Station for Subtropical Forest Ecosystem Research Studies (ASSFERS, 24°32′N, 101°01′E, 2476 m elevation), Yunnan province, Southwest China. Details of this forest ecosystem have been presented in our previous work.[17,24,25,41−43] Briefly, ASSFERS has a subtropical climate with a canopy level dominated by old-growth (stand age >300-year) and evergreen beech tree species, such as *Lithocarpus xylocarpus* (LX), *Castanopsis wattii* (CW), and *Schima noronhae* (SN).[44] ASSFERS is dominated by alfisols, with a pH of 3.55−3.95 in the topsoil.[42] At the station, which is part of the global mercury observation system (GMOS) network, for 2014, an average value of 1.4 ± 0.3 ng m^{-3} was reported for Hg^0 in air,[29] which categorizes it as a background site.[45] In addition, the concentration of the particle-bound mercury (PBM) and gaseous oxidized mercury (GOM) in air is typically below 40 and 5 pg m^{-3}, respectively.[29] A square-shape, undisturbed plot (30 × 30 m^2) was utilized for experiments which were then divided into two subplots (A and B) for measurements of soil pore gas (A) and air−soil gas exchange (B) as previously described.[42]

2.2. Stable Hg Isotope Sampling in Soil Pore Gas. The methodology of sample collection for Hg^0 isotope analysis in the soil pore gas has been described elsewhere.[42] Briefly, the modified centrifuge tubes, with fifty holes of 1.5 mm diameter on one side, were horizontally inserted into the undisturbed 10 cm-deep soil profile. The horizontal distance between the two centrifuge tubes was 50−60 cm. Thirty tubes divided into five groups with Teflon tees were applied to sample the soil pore gas (Figure S1).[42] We sampled soil pore gas at sub-site A during April 2018 (spring), July 2019 (summer), October to November 2019 (autumn), and January 2020 (winter). Each seasonal sampling was conducted for four to five days except during the winter when up to ten days were required to obtain robust samples. Three replicate samples were collected during each season.

Given the reported Hg^0 concentration in soil pore gas (3.5−13.3 ng m^{-3}),[42] the soil pore gas was pumped into 0.4 g of chlorine-impregnated activated carbon (ClC) traps[46] with a flow rate of 0.5 L min^{-1} during extensive time to ensure sufficient amount of Hg^0 (>5 ng) is collected (detailed in Supporting Information, Section 1, and illustrated in Figure S1). The flow rate of 0.5 L min^{-1} has been shown to adequately concentrate Hg^0 for stable isotope analysis in our experiments[42] (Table S1). To compensate for the low sampling flow rate (0.5 L min^{-1}), 0.4 g of ClC material per trap (system blank: 196 ± 23 pg g^{-1}, which is below 100 pg in each trap) was applied to ensure a low system blank. The Hg^0 concentration in soil pore gas was monitored intermittently for 1 h per day during isotope sampling by a direct-indicating instrument (Tekran model 2537X, shown in Table S1). The monitoring indicated that the Hg^0 concentration was relatively stable over the measurement period with a maximum reduction of less than 15% of the initial values after 96−120 h.[42]

2.3. Stable Hg Isotope Sampling during Air−Soil Hg^0 Exchange. The air−soil Hg^0 exchange experiments under ambient air and Hg-free air exposure were carried out seasonally during 2017−2018 with more detailed information supplied in Table S2. Exposure by Hg-free air was used for eliminating Hg^0 uptake into the soil and therefore only measuring the unidirectional flux of Hg^0 from the soil. The experimental setup as well as flux data excluding isotope measurements for chamber exposure to ambient air have been reported earlier.[42] Bidirectional air−soil Hg^0 exchange was measured over three randomly selected forest floor plots in the vicinity of LX, CW, and SN plants. We utilized traps containing the 0.8 g ClC material to sample both the inlet and the outlet of an aerodynamically designed DFC (aero-DFC) for isotope analysis of gaseous Hg^0[47,48] using a flow rate of 8−10 L min^{-1} (illustrated in Figure S2).[46] The aero-DFC described in Lin et al.[48] was modified so that a high flow (10−12 L min^{-1}) of Hg-free (zero) air could be appropriately introduced over enclosed soil (Figure S2). As a source of the Hg-free purging air (<20 pg Hg^0 m^{-3} n, Table S3), a Teflon-lined pump (model N860ATE, KNF Neuberger, Germany) with an upstream-mounted air scrubber was used (Zero canister, Tekran). Over a sampling period of 4−5 days, we were able to obtain two flux samples for exposure to ambient air and one flux sample for exposure to Hg-free air by using two aero-DFCs.

2.4. Stable Hg Isotope Measurements. All exposed ClC-traps were processed by using double-stage heating pyrolysis in a tube muffle furnace[49] to pre-concentrate the analyte into 5 ml oxidizing solution of 40% mixture of concentrated nitric and hydrochloric acid ("reverse aqua regia", $HNO_3/HCl = 2:1$, v/v). The oxidizing solution was analyzed for Hg by cold vapor atomic fluorescence spectrometry (model 2500, Tekran Instruments, Canada) following the steps prescribed by the US-EPA method 1631 (detection limit: 0.5 ng L^{-1}).[50] The pre-concentration recovery was determined to be 94.2 ± 1.5% ($\pm 1\sigma$, $n = 6$) using a BCR standard reference material (BCR-482, 480 ± 20 ng Hg g^{-1}), 94.4 ± 3.8% for ClC-trap samples in laboratory experiments using the vapor Hg^0 source (Tekran 2505) as methodology of Fu et al.,[46] and 97.5 ± 6.9% for all ClC-trap samples in field samples (detailed in Supporting Information, Tables S2 and S5−S7).

Hg isotope compositions were measured by a multi-collector inductively coupled plasma mass spectrometer (MC-ICPMS, Neptune II, Thermo Scientific, USA) at the State Key Laboratory of Ore Deposit Geochemistry, Institute of Geochemistry, Chinese Academy of Sciences, Guiyang. The sample introduction system for Hg isotope ratio measurements consists of an online Hg generation system[51] (HGX-200, Teledyne CETAC Technologies, USA) coupled to a CETAC Ardius II Desolvating Nebulizer System as described in earlier studies.[24,52] Following the calculation from Bergquist and Blum,[40] MDF is reported as

$$\delta^{202}\mathrm{Hg}(‰) = [(^{202}\mathrm{Hg}/^{198}\mathrm{Hg})_{\mathrm{sample}}/(^{202}\mathrm{Hg}/^{198}\mathrm{Hg})_{\mathrm{ref}} - 1] \times 1000 \quad (1)$$

MIF is calculated as

$$\Delta^{xxx}\mathrm{Hg}(‰) = \delta^{xxx}\mathrm{Hg} - \delta^{202}\mathrm{Hg} \times \beta_{xxx} \quad (2)$$

where β_{xxx} is 0.252 for ^{199}Hg, 0.502 for ^{200}Hg, and 0.752 for ^{201}Hg, respectively. $(^{202}Hg/^{198}Hg)_{ref}$ represents such a result in the standard sample, Nist 3133.

2.5. Mercury Mass Balance Model. An isotopic mass balance model was applied to measurement data aiming to budget the contribution of the individual flux components. The model is based on the following assumptions (more details in the next section): (1) samples taken during the winter by zero air exposure and under sunlight determine the photoreduction-mediated flux endmember isotopically as detailed in Section 3.2, (2) pore gas emission introduces a negative MDF shift in Hg^0 that is ventilated to air without affecting odd-MIF,[53] and (3) gross Hg^0 deposition does not lead to odd-MIF transition, as illustrated by the Hg isotopic signatures of winter Hg^0 exchange, as described in Section 3.3. Finally, the calculation of the bi-directional net Hg^0 exchange between soil and the atmosphere is accomplished by summing up contributions from atmospheric Hg^0 gross deposition, topsoil photo-reduction sourced emission, and Hg^0 pore emission from soil into air.[7,42,54,55] Hence, the following mass balance equations can be established

$$M_{\mathrm{inlet}} + M_{\mathrm{pho}} + M_{\mathrm{emi}} = M_{\mathrm{outlet}} + M_{\mathrm{dep}} \quad (3)$$

$$M_{\mathrm{inlet}}\cdot\Delta^{xxx}\mathrm{Hg}_{\mathrm{atm}} + M_{\mathrm{pho}}\cdot\Delta^{xxx}\mathrm{Hg}_{\mathrm{pho}} + M_{\mathrm{emi}}\cdot\Delta^{xxx}\mathrm{Hg}_{\mathrm{emi}} = M_{\mathrm{outlet}}\cdot\Delta^{xxx}\mathrm{Hg}_{\mathrm{exc}} + M_{\mathrm{dep}}\cdot\Delta^{xxx}\mathrm{Hg}_{\mathrm{atm}} \quad (4)$$

$$M_{\mathrm{pho}}\cdot\Delta^{xxx}\mathrm{Hg}_{\mathrm{pho}} + \xi\cdot M_{\mathrm{emi}}\cdot\Delta^{xxx}\mathrm{Hg}_{\mathrm{emi}} = (M_{\mathrm{pho}} + \xi\cdot M_{\mathrm{emi}})\cdot\Delta^{xxx}\mathrm{Hg}_{\mathrm{zero\text{-}exc}} \quad (5)$$

where *xxx* represents Hg isotopes with mass number 199 or 201. M_{inlet}, M_{outlet}, M_{dep}, M_{pho}, and M_{emi} represent the Hg^0 flux entering the DFC from the ambient air, exiting the DFC, removed by gross deposition, supplied by photo-reduction-sourced emissions and by gas emanating by pore emission, respectively (unit: ng m^{-2} h^{-1}). $\Delta^{xxx}Hg_{atm}$, $\Delta^{xxx}Hg_{pho}$, $\Delta^{xxx}Hg_{emi}$, $\Delta^{xxx}Hg_{exc}$, and $\Delta^{xxx}Hg_{zero\text{-}exc}$ represent Hg^0 odd-MIF signatures of near-surface ambient air, of topsoil influenced by photo-reduction, of soil pore gas, of ambient air exchange flux and of the efflux deriving from zero-air exposures, respectively (unit: ‰) (Section 2 of Supporting Information). ξ is a correction factor to offset the increased emission-driven change in the data collected with Hg-free air. Equations 3 and 4 are based on the Hg isotopic mass balance during the air−soil Hg^0 exchange under ambient air exposure. Equation 5 is based on the Hg isotopic mass balance during Hg^0 evasion under ambient air exposure. The model structure and parameter settings are detailed in Supporting Information, Section 2.

2.6. Quality Assurance/Quality Control and Statistical Analysis. During the whole experiment, we have conducted strict quality assurance (QA)/quality control (QC) and the detailed information can be found in Section 3 of Supporting Information. Statistical methods are described with the data provided in the text. Correlations between Hg^0 flux and isotopic signatures were obtained by Pearson's correlation tests using SPSS software (SPSS 20.0). The differences in the correlation coefficient are determined using a significant level of 0.05 if not otherwise stated.

3. RESULTS AND DISCUSSION

3.1. Sources of Hg^0 in Soil Pore Gas and Underlying Mechanisms. Soil acts as both a source and sink for Hg^0 in near-surface air depending on the Hg^0 concentration in pore gas.[5,9,10] We have reported the time series of Hg^0 concentrations measured in pore gas,[42] which exhibits a distinct seasonal pattern. High and varying concentrations were observed during spring (11.9 ± 4.7 ng m^{-3}), summer (17.6 ± 15.9 ng m^{-3}), and autumn (5.0 ± 2.8 ng m^{-3}). The concentrations observed in winter were comparatively low and consistent (2.2 ± 0.9 ng m^{-3}, Table S2). The factors driving the seasonal variation have been attributed to soil temperature and soil water content.[42] The former speeds up the rates of both microbial and abiotic reduction processes that contribute to higher levels of Hg^0 in the pore gas as well as the pore diffusion rate of Hg^0.[9,42] In turn, the soil water content restricts the space available for gas in the pores, hence inhibiting soil pore Hg^0 concentration and lowering the pore diffusivity.[42,56] Variations in atmospheric pressure, on the other hand, have an undetectable effect on the soil pore Hg^0 level. Although Hg^0 is a small atom compared to typical gas molecules, it is significantly more polarizable than many other trace gases,[57] suggesting interaction with, for example, π-system moieties[58] of NOM and some degree of retention to soil particles.[59,60] In addition to sorption on soil surfaces, Hg^0 in pore gas is controlled by the redox chemistry and pore diffusion driven by concentration gradients.[9,18,33−35,37] Since sunlight penetrates <1 cm into the forest floor,[61,62] Hg^0 produced in the photic zone of the O-horizon makes little contribution to the Hg^0

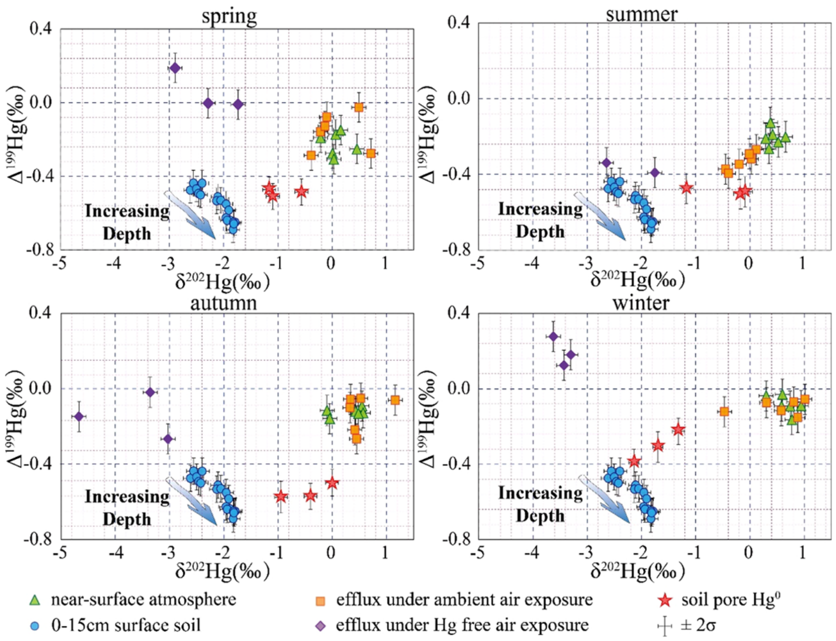

Figure 1. Observed Hg isotopic compositions (Δ^{199}Hg vs δ^{202}Hg) in aerial compartments and surface soil during air−soil Hg exchange flux of the ASSFERS forest ecosystem. The surface soil profile (blue filled circles) isotopic data were from Yuan et al.,[17] which is near the experiment plot. The blue arrows associated with "Increasing Depth" indicate the positive direction for MDF and negative direction for odd-MIF during soil depth increasing from 0 to 15 cm.[17] The experiments occurred at different seasons are marked at the top of each scatterplot. The measured endmembers are marked at the bottom of the scatterplot. The error bars represent ±2 standard deviation.

pool in pore gas sampled at a depth of 10 cm but representing a mixture from the organic soil profile.

In the present work, the isotopic signatures in soil pore Hg^{0} are determined to be δ^{202}Hg = −0.94 ± 0.32‰, Δ^{199}Hg = −0.49 ± 0.04‰ and Δ^{200}Hg = −0.03 ± 0.05‰ ($n = 3$, 1σ) for spring; δ^{202}Hg = −0.48 ± 0.60‰, Δ^{199}Hg = −0.49 ± 0.04‰ and Δ^{200}Hg = −0.02 ± 0.05‰ ($n = 3$, 1σ) for summer; δ^{202}Hg = −0.45 ± 0.47‰, Δ^{199}Hg = −0.55 ± 0.04‰ and Δ^{200}Hg = −0.05 ± 0.05‰ (n = 3, 1σ) for autumn; and δ^{202}Hg = −1.72 ± 0.41‰, Δ^{199}Hg = −0.31 ± 0.08‰ and Δ^{200}Hg = −0.03 ± 0.05‰ ($n = 3$, 1σ) for winter (Figure 1 and Table S2). The isotope signals among spring, summer, and autumn (Figure 1 and S3) are not significantly different ($p > 0.05$, ANOVA test), but differ significantly for both δ^{202}Hg and Δ^{199}Hg compared to those of winter samples ($p < 0.01$, ANOVA test).

In a comparison with soil pore Hg^{0}, Hg^{0} in near-surface air samples ($n = 24$) is isotopically characterized by more positive values in MDF (δ^{202}Hg = 0.37 ± 0.30‰) and odd-MIF (Δ^{199}Hg = −0.16 ± 0.07‰) but the pools exhibit insignificant Δ^{200}Hg (−0.05 ± 0.04‰). In turn, ASSFERS soil δ^{202}Hg signature increases with depth from −2.61‰ on surface to −1.79‰ in soil at 15 cm deep, with soil Δ^{199}Hg signature displaying a corresponding decrease with depth from −0.44 to −0.69‰[17] (outlined in Figure 1). The Δ^{199}Hg signatures in soil pore gas in spring, summer, and autumn are comparable to the signatures of surrounding soil down to a depth of 15 cm, but δ^{202}Hg is 1−2‰ more positive in the gas compared to the surrounding soil. Interestingly, the δ^{202}Hg values of soil pore gas during winter are similar to those of soil Hg, but the corresponding Δ^{199}Hg values are shifted by nearly +0.2‰.

One explanation for the similar Δ^{199}Hg but more positive δ^{202}Hg values in the pore gas compared to the surrounding soil from spring to autumn is a combination of: (1) strong Hg^{0} emission driven by the concentration gradient from the soil pore gas (4.6−23.6 ng m^{-3}) to ambient air (0.80−2.2 ng m^{-3}) and (2) Hg^{0} emission induced by soil water evapotranspiration[56,63] (detailed in Section 3.4). The outgoing Hg emission leads to heavier Hg^{0} isotopes in the soil pore. This phenomenon is further supported by the more negative δ^{202}Hg in Hg efflux under the Hg-free air than those in the soil pore gas (Figure 1). Mean δ^{202}Hg^{0} values of these atmospheric Hg^{0} sources are broken down by season as follows: −2.30 ± 0.58, −2.20 ± 0.63, and −3.69 ± 0.87‰ in the soil efflux gas versus −0.94 ± 0.32, −0.48 ± 0.60, and −0.45 ± 0.47‰ in the soil pore gas for spring, summer, and autumn, respectively. Analogous to proven strong MDF during Hg^{0} emission in small-bore tubes,[53] upward emission may drive the remaining Hg^{0} toward more positive δ^{202}Hg values despite that oxidation, reduction, and desorption act in the negative MDF direction on the Hg^{0} pool in the porous soil. We found comparable Δ^{199}Hg values in the pore gas and in the surrounding soil at the same depth during spring to autumn. Microbial reduction occurs without the odd-MIF shift,[33,34] and abiotic Hg dark reduction induced by organic matter causes a small odd-MIF shift[17,18,64] with an enrichment factor of 0.18.[37] It is plausible that the pore gas Hg^{0} comes from a mixture of Hg microbial reduction and abiotic dark reduction and few atmospheric Hg^{0} deposition during the spring, summer, and autumn seasons.

Although Hg^{0} concentration in the soil pore gas (∼2.2 ng m^{-3}) was higher than the value observed in the ambient air (0.8−0.9 ng m^{-3}) in winter, Hg^{0} deposition onto soil clearly occurred despite the concentration gradient favoring Hg^{0} evasion from soil (discussed in detail in Section 3.4). During winter, the changed isotope composition relative to that of surrounding soil indicates an influx of Hg^{0} from ambient air since air Δ^{199}Hg has a more positive value. This makes the isotopic signature in pore gas closer to that in near-surface air (δ^{202}Hg = 0.66 ± 0.22‰ and Δ^{199}Hg = −0.08 ± 0.05‰). Furthermore, the pore air exhibits a Δ^{199}Hg/Δ^{201}Hg ratio of unity (1.00 ± 0.13, Figure 2) indicating that this Hg^{0} pool has air[65] or microbial reduction as its source rather than abiotic dark reduction associated with a larger ratio.[37]

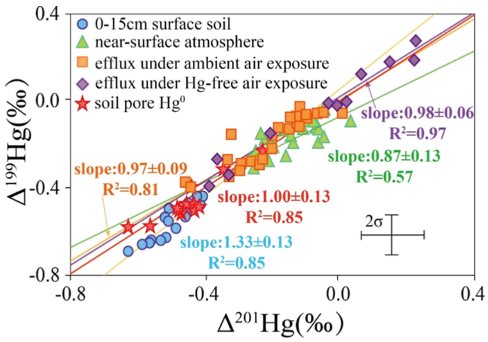

Figure 2. Mass-independent fractionation of odd isotopes (Δ^{199}Hg vs Δ^{201}Hg) of Hg^0 in near-surface atmosphere (green filled triangles), in efflux gas of aero-DFC under ambient air exposure (orange filled squares), in efflux gas of aero-DFC under Hg-free air exposure (purple filled diamonds), in soil pore gas (red filled stars), and Hg^{II} in 0−15 cm surface soil (blue filled circles). The surface soil profile of isotopic data are from Yuan et al[17] Linear fits are obtained from the Williamson-York bivariate regression method.[80] Each slope is marked with one standard error of the mean in corresponding color. The error bar given in bottom right represents ±2 standard deviation.

3.2. Isotope Characteristics for Evasion of Hg^0 Stored on Forest Floor.

The observed Hg^0 evasion flux over soil under Hg-free air exposure are shown in Table S3. The flux (range: 0.21−3.83 ng m^{-2} h^{-1}) features a diurnal pattern related to temperature and solar radiation at noon (Figures S4−S6). Seasonally, each of the three plots examined in such Hg-free air exposure shows higher Hg^0 emissions during spring and summer than during autumn and winter (Table S3).

The efflux Hg^0 in the outlet of the flux chamber under Hg-free gas shows considerable seasonal variation in both Δ^{199}Hg (range from −0.39 to 0.28‰) and δ^{202}Hg (range from −4.67 to −1.73‰) signatures (Figure 1 and Table S5). The evading Hg^0 is derived from photo-reduction that occurred at the surface floor and Hg^0 emission through the porous organic soil when exposed to zero air, as indicated by the observed Δ^{199}Hg/Δ^{201}Hg of 0.98 ± 0.06 (R^2 = 0.97). Unlike the data reported elsewhere, the Hg^0 effluxes measured during the winter in the vicinity of *Schima noronhae* and *Lithocarpus xylocarpus* show nearly zero flux most of the day when light is limited (Figures S4 and S5). This suggests that the contribution of pore gas Hg^0 emission can be neglected. The isotopic shifts of the Hg^0 efflux under Hg-free gas exposing between daytime and light in winter are likely caused by the surface soil Hg photoreduction. An earlier study has depicted that 33% reduction is caused by organosulfur photoreduction, 6% reduction by photoreduction mediated by organic matter, and ~60% by microbial reduction on the forest surface floor at ASSFERS.[17] Considering the Hg odd-MIF during each reduction processes, the photoreduction-induced Hg^0 efflux can cause 0.20−0.23‰ of Δ^{199}Hg (Supporting Information Section 3). This is consistent with the average value of Δ^{199}Hg for winter Hg^0 efflux under Hg-free gas exposing (Δ^{199}Hg = 0.23 ± 0.04‰ and Δ^{201}Hg = 0.19 ± 0.04‰). Therefore, the values of 0.23 and 0.19‰ for $\Delta^{199}Hg_{pho}$ and $\Delta^{201}Hg_{pho}$ are applied in eqs 3−5.

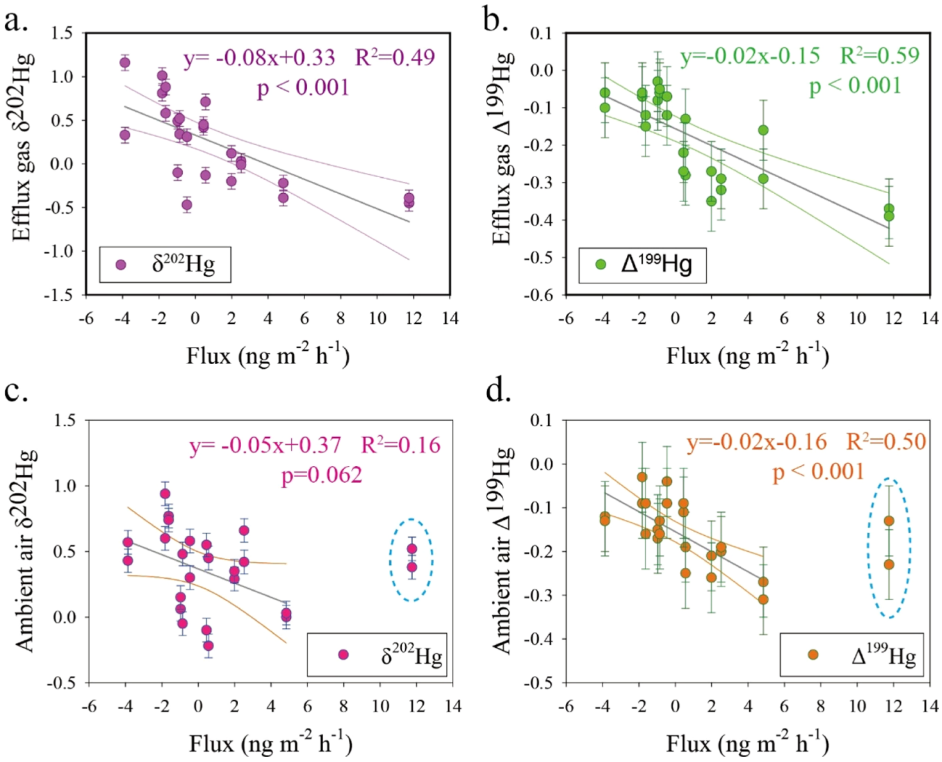

Figure 3. Scatterplot of isotopic signatures vs Hg^0 flux from all aero-DFC experiments under ambient air exposure. (a) δ^{202}Hg vs flux, (b) Δ^{199}Hg vs Flux in the efflux gas of aero-DFC, (c) δ^{202}Hg vs Flux, and (d) Δ^{199}Hg vs Flux in near-surface ambient air. Error bars indicate ±2 standard deviations. The straight lines represent the regression fitting results, and the envelopes represent the 95% confidence interval. The dotted line encircled points that are not included in the present fit line in (c,d).

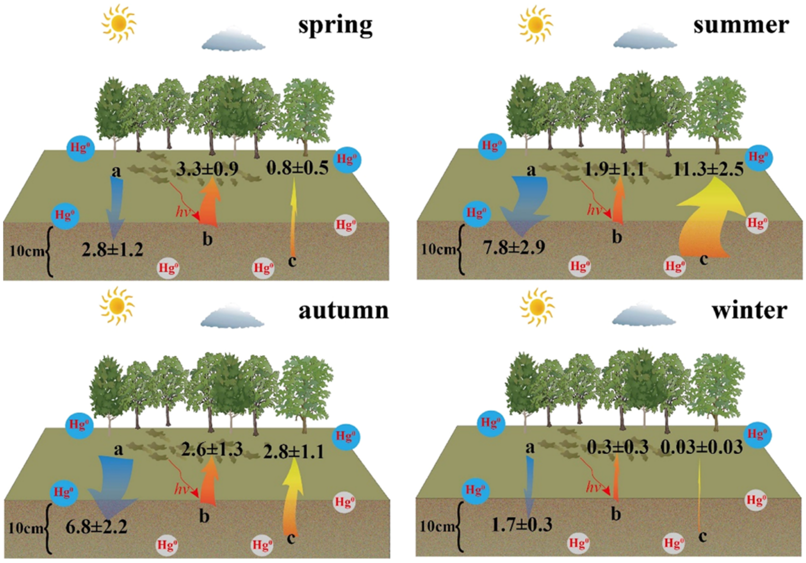

Figure 4. Model results on the contribution flux in the air−soil Hg^0 exchange process. Flux unit: ng m^{-2} h^{-1}. Inlaid arrows represent the atmospheric Hg^0 gross deposition for a filled in blue, the surface soil Hg^{II} photoreduction for b filled in orange, and Hg^0 emission from deeper soil for c filled in yellow, respectively.

As seen in Figure 1, summertime Hg^0 efflux data form a cluster (δ^{202}Hg = −2.20 ± 0.63‰ and Δ^{199}Hg = −0.36 ± 0.07‰) much closer to that of the organic soil horizon (δ^{202}Hg = −2.23 ± 0.27‰ and Δ^{199}Hg = −0.52 ± 0.06‰) with respect to Δ^{199}Hg and δ^{202}Hg than is the case in other seasons. Corresponding negative-shifted odd-MIF signatures (Δ^{199}Hg = −0.36 ± 0.07‰ and Δ^{201}Hg = −0.36 ± 0.09‰) are also considerably similar to those of the pore gas (Δ^{199}Hg = −0.49 ± 0.04‰ and Δ^{201}Hg = −0.46 ± 0.14‰). In turn, the isotopically lighter efflux relative to the pore gas is an effect of MDF caused by emission. The contribution of photoreduction on efflux is weaker because of the more intensive canopy shading constraining the sunlight breakthrough into the forest floor.[66] The observed isotopic signatures in Hg^0 efflux are largely controlled by pore Hg^0 gas emission through the organic matter in soil, which is also evidenced by the higher evasion flux (Figures 1 and S3).[42] When all samples for Hg^0 efflux and Hg^0 in pore gas are plotted in the odd-MIF versus MDF space, a linear relationship is evident with a slope for Δ^{199}Hg/δ^{202}Hg and Δ^{201}Hg/δ^{202}Hg of −0.57 ± 0.07 and −0.53 ± 0.07, respectively (Figure S7). The significant relationship ($p < 0.01$) represents a binary mixing of Hg^0 derived from surface photoreduction and from pore gas.

3.3. Process of the Air−Soil Hg^0 Exchange Indicated by Hg Isotopic Evidence. Air−soil Hg^0 net exchange (F_{Hg}) measured by the aero-DFC (detailed in Supporting Information Section 3 of Yuan et al.[42]) shows continuous deposition (−0.46−−1.82 ng m^{-2} h^{-1}) in winter and continuous emission (1.99−11.75 ng m^{-2} h^{-1}) in summer, while the spring and autumn measurements contain periods of deposition but predominantly emission (−0.97−4.84 ng m^{-2} h^{-1}). Overall, the forest floor is a net Hg^0 source with an annual flux of +6.7 ± 20.5 μg m^{-2} yr^{-1}.[42] Temperature is the most important factor driving the air−soil Hg^0 exchange, followed by air Hg^0 concentration.[42]

The isotopic signatures in the air−soil Hg^0 net exchange show seasonal variability (Figures 1 and S8 and Tables S6 and S7). During the winter, there is insignificant difference (paired *t*-test, $p = 0.445$ for δ^{202}Hg and $p = 0.486$ for Δ^{199}Hg) between ambient air entering (δ^{202}Hg = 0.66 ± 0.22‰ and Δ^{199}Hg = −0.08 ± 0.05‰, $n = 3$, Table S6) and exiting (δ^{202}Hg = 0.52 ± 0.55‰ and Δ^{199}Hg = −0.10 ± 0.04‰, $n = 3$) through aero-DFC, while during the summer (paired *t*-test, $p < 0.01$), the outgoing air modified by the gas exchange is more negative (δ^{202}Hg = −0.15 ± 0.23‰ and Δ^{199}Hg = −0.33 ± 0.05‰, $n = 3$) compared to the ambient air (δ^{202}Hg = 0.43 ± 0.13‰ and Δ^{199}Hg = −0.20 ± 0.05‰, $n = 3$). Also, the difference in isotope compositions during spring and autumn is insignificant (paired *t*-test, all $p > 0.05$). Similar to the air samples collected at ASSFERS and other forest sites in China, the flux measured by the DFC method yields a Δ^{199}Hg/Δ^{201}Hg ration close to unity (0.97 ± 0.09 and 0.87 ± 0.13, respectively). This is in contrast to that of Hg bound in the soil profile being shaped by the nuclear volume effect during thermal reduction.[17]

The isotopic signatures of outgoing air modified by the gas exchange over the plot enclosed in the chamber show a significant linear anticorrelation ($p < 0.001$) with F_{Hg} (in the range from −1.82 to 11.75 ng m^{-2} h^{-1}, $n = 12$) expressed in the form $-0.08F_{Hg} + 0.33$ ($R^2 = 0.49$) and $-0.02F_{Hg} - 0.15$ ($R^2 = 0.59$) for δ^{202}Hg and Δ^{199}Hg, respectively (Figure 3a,b). Since the near-surface air into the DFC is often isotopically similar to the outgoing air, there is an anticorrelation with the former and F_{Hg} (Figure 3c,d). Based on the analysis in Section 3.2, the net Hg^0 flux between soil and air is determined as the result of a ternary mixing process among gross deposition, photo-reduction in the topsoil mediated by organosulfur-containing ligands and by emission-ventilated pore gas. However, the anticorrelation can also be caused by an increasing relative contribution of soil emission to near-surface ambient air, which leads to the isotopic signatures similar to those observed in soil pore gas with negative MDF and odd-MIF.

3.4. Sources of Hg^0 Contributing to the Air−Soil Hg^0 Fluxes. Results from model simulations for each season are presented in Figure 4. The simulated M_{dep} normalized for the soil surface enclosed by the chamber is highest in summer (7.8 ± 2.9 ng m^{-2} h^{-1}), followed by autumn (6.8 ± 2.3 ng m^{-2} h^{-1}), spring (2.8 ± 1.2 ng m^{-2} h^{-1}), and winter (1.7 ± 0.3 ng

m^{-2} h^{-1}), consistent with a declining trend for the Hg^0 level in near-surface air from 1.81 ± 0.46 in summer to 0.86 ± 0.13 ng m^{-3} in winter[42] (Figure S9). The simulated M_{emi} increases from 0.03 ± 0.03 ng m^{-2} h^{-1} in winter to 11.3 ± 2.5 ng m^{-2} h^{-1} in summer (Figure 4). Finally, the simulated photoreduction-driven flux also varies in the following order: 0.3 ± 0.3 ng m^{-2} h^{-1} (winter) < 1.9 ± 1.1 ng m^{-2} h^{-1} (summer) < 2.6 ± 1.3 ng m^{-2} h^{-1} (autumn) < 3.3 ± 0.9 ng m^{-2} h^{-1} (spring). The highest value in spring is consistent with the highest annual observations of photosynthetically active radiation below the canopy (40−52 μE m^{-2} s^{-1}).[42] Our isotope mass balance model suggests that legacy Hg re-emission (∼50 ± 41 μg m^{-2} yr^{-1}) plays an important role in the air−soil Hg^0 exchange at ASSFERS, with an estimated contribution of 17 ± 17 μg m^{-2} yr^{-1} by photoreduction-driven emission and 33 ± 25 μg m^{-2} yr^{-1} of Hg^0 emanating from the organic soil horizon by pore emission.

Hg^0 deposition through litterfall has been considered as an important pathway of dry deposition in forest ecosystems.[13,14] We applied a mass balance model based on measured Hg isotopes and estimated the gross air Hg^0 deposition to forest floor to be −4.7 ± 3.8 ng m^{-2} h^{-1} (−42 ± 33 μg m^{-2} yr^{-1}) accounting for approximately 60% of Hg in the litterfall flux at ASSFERS (∼75 μg m^{-2} yr^{-1}).[66,67] This suggests that using only litterfall flux to represent the total dry deposition significantly underestimates the total Hg^0 dry deposition to forest ecosystems. We attributed the large observed Hg^0 dry gross deposition to the deposited Hg^0 being rapidly adsorbed and oxidized into Hg^{2+} in the surface organic soil layer due to the high level of reduced sulfur or N/O functional groups.[15,35,66] The adsorption induced the ∼−0.4‰ enrichment factor of lighter Hg isotopes into the adsorbed state which was independent of the equilibration time and fraction.[68] The pseudo-first-order oxidation rate of Hg^0 has been observed to be up to 5.4 h^{-1} for N/O-mediated redox reaction and 0.14 h^{-1} for thiol compounds redox.[69,70]

Figure S12 further explains the conceptual model of the air−soil Hg^0 exchange. Absorption and oxidation in the surface soil layer are the primary drivers for the gross deposition. Diffusion between air and soil pores and soil water evapotranspiration induce soil pore Hg^0 evasion. During spring, summer, and autumn, the deposition flux driven by chemisorption from air to soil is 1−2 orders of magnitude greater than the values predicted by static diffusion using the Fick's first law. This highlights the importance of the absorption and oxidation process on the soil surface. The emission from the soil pore to air is also 2−30 times higher than the value explained by diffusion, because other processes such as the soil water evapotranspiration facilitates the gross emission in these warm seasons.[56,63,71] The total gross emission from the soil pore to air is also 1−2 orders of magnitude higher than the gross deposition from the air to soil pore, consistent with the observed trend of Hg^0 odd-MIF signatures. In winter, the total gross emission from the soil pore to air is largely reduced because of the much-reduced rate of formation and diffusion of pore Hg^0 and the soil water evapotranspiration under low temperatures.[56,63] This yields a more positive value of the pore Hg^0 odd-MIF signatures, similar to the signatures of air Hg^0.

3.5. Model Uncertainties.

The uncertainties of the model estimates come primarily from a lack of comprehensive understanding of processes that contribute to the MIF shifts. First, the MIF caused by atmospheric Hg^0 absorption and dark oxidation, both being important pathways to fix deposited Hg^0 in organic soil, are close and inseparable in model parameterization. Given the nearly zero odd-MIF shift occurred at absorption and the small positive odd-MIF shift caused by dark oxidation,[35,36] there was no odd-MIF transition in our experiment with net deposition flux during winter. Another source of uncertainties arises from the potentially unknown processes taking place in soil profiles. For example, the photoreduction induced by large organic molecules and the Hg^0 absorption onto organic soils were not incorporated in the present model. In essence, the negative odd-MIF shift in product Hg^0 can also be caused by photoreduction mediated by organic matter.[38,40] Since the photoreduction induced by large organic matter molecules contribute to <6% of total soil Hg reduction,[17] the induced odd-MIF shift in product Hg^0 is not considered in the model. Data quantifying the MIF shift during Hg^{II} absorption onto organic matter molecules[68,72] are not available, and therefore, the soil pore gas Hg^0 signature represents the endmember of the emission process. Finally, the sensitivity analysis in Figure S13 suggests that the soil pore-to-air emission flux is more dependent on the variation of gross atmospheric Hg^0 deposition flux than the surface Hg^{II} photereduction flux. This indicates that not-yet-identified processes could lead to the current Hg isotopic mass balance model under-constrained, especially for estimating the soil pore to air Hg^0 evasion flux.

Uncertainty is also introduced from the Hg isotopic signatures used for the endmembers. The values used in the model represent mean values that potentially eliminate process signals. For example, the specific isotopic signatures of Hg in soil pore gas in spring, summer, and autumn are applied in each season during simulation, while the winter soil pore Hg^0 is expected to be impacted by the atmospheric Hg^0 mixing and oxidation. The mean value of odd-MIF in other seasons was applied in winter simulation. In addition, although the observed Hg isotopic signatures in near-surface ambient air at the ASSFERS[23−25] and other remote sites are consistent,[19,27,30] the true atmospheric Hg^0 isotopic signatures without being modified by the air−soil exchange was not independently quantified. We found that using the inlet Hg^0 compositions to represent the signature of atmospheric Hg^0 endmember is reasonable. Little difference (1−3%, Figure S11) was observed with the mean atmospheric Hg^0 isotopic compositions at ASSFERS (Δ^{199}Hg = −0.13 ± 0.08 and Δ^{201}Hg = −0.12 ± 0.08‰[23−25]) as the model input. We recommend more studies to demonstrate these unknown mechanisms of soil Hg biogeochemical processes for future modeling updates.

4. IMPLICATIONS

Few studies have quantified the multi-process contribution during the air−soil Hg^0 exchange because of the limitations of measurement methodology that is capable of quantifying the net flux only. In this study, the processes contributing to the bi-directional exchange has been quantitatively attributed based on the stable isotope data of Hg. Currently, the net flux exchanged between atmosphere and forest ecosystems is estimated to be 151 Mg yr^{-1} (range: 97−247 Mg yr^{-1}) globally.[2,3,73−76] These estimates ignore contribution from intermediate Hg processes in forest ecosystems, especially the role of legacy Hg re-emission. We calculated that ∼11.5 μg m^{-2} yr^{-1} Hg^0 was emitted from Hg deposition on foliage,[24,42] and the legacy Hg re-emission from forest floor is estimated up to ∼50 ± 41 μg m^{-2} yr^{-1} in the present study. The relatively large uncertainties need more observation and isotopic data to quantify in future. This study demonstrates a new methodology in estimating Hg^0 exchange fluxes derived from various pathways on the forest floor with the observed characteristics of Hg stable isotopes and provides data of Hg stable isotopes in different soil compartments. The new findings facilitate a better understanding of Hg cycling in forest ecosystems. The negative transition in both MDF and odd-MIF during soil-air Hg exchange offsets the positive shift in those during the foliage-air Hg exchange, maintaining the stability of the atmospheric Hg^0 isotopic feature.

The slightly negative (−0.2−−0.1‰) odd-MIF signatures of atmospheric Hg^0 have been reported at multiple remote sites[19,22−27] and cannot be explained by the near-zero odd-MIF signatures observed in air samples of anthropogenic Hg release[32,77−79] and positive odd-MIF shifts after experiencing the air-foliage bi-directional exchange.[24] It is likely that the negative odd-MIF is forced by the evasion of Hg stored in the surface forest floor layer. More studies on legacy Hg reemission with Hg isotopic signatures in other ecosystems are needed to improve our understanding of global cycling of Hg mass.

■ ASSOCIATED CONTENT

Supporting Information

The Supporting Information is available free of charge at https://pubs.acs.org/doi/10.1021/acs.est.1c02744.

> Additional experimental details, materials, data sets and methods, including the experimental setup, flux results, and Hg isotopic mass balance model, sketch of setup for soil pore gas Hg^0, seasonal Hg isotopic compositions, diurnal variations, $\Delta^{199}Hg$ and $\Delta^{201}Hg$ versus $\delta^{202}Hg$ in efflux gas and soil pore gas, observed Hg isotopic compositions, scatterplot, model-simulated specific flux, conceptual model of the air-soil Hg^0 exchange, and sensitivity analysis (PDF)

■ AUTHOR INFORMATION

Corresponding Author

Xinbin Feng − *State Key Laboratory of Environmental Geochemistry, Institute of Geochemistry, Chinese Academy of Sciences, Guiyang 550081, China; Center for Excellence in Quaternary Science and Global Change, Chinese Academy of Sciences, Xi'an 710061, China;* orcid.org/0000-0002-7462-8998; Phone: 86-851-85895728; Email: fengxinbin@vip.skleg.cn

Authors

Wei Yuan − *State Key Laboratory of Environmental Geochemistry, Institute of Geochemistry, Chinese Academy of Sciences, Guiyang 550081, China; University of Chinese Academy of Sciences, Beijing 100049, China*

Xun Wang − *College of Resources and Environment, Southwest University, Chongqing 400715, China;* orcid.org/0000-0002-7407-8965

Che-Jen Lin − *Center for Advances in Water and Air Quality, Lamar University, Beaumont, Texas 77710, United States*

Jonas Olof Sommar − *State Key Laboratory of Environmental Geochemistry, Institute of Geochemistry, Chinese Academy of Sciences, Guiyang 550081, China;* orcid.org/0000-0001-8634-440X

Bo Wang − *State Key Laboratory of Environmental Geochemistry, Institute of Geochemistry, Chinese Academy of Sciences, Guiyang 550081, China; University of Chinese Academy of Sciences, Beijing 100049, China*

Zhiyun Lu − *National Forest Ecosystem Research Station at Ailaoshan, Jingdong, Yunnan 676209, China*

Complete contact information is available at: https://pubs.acs.org/10.1021/acs.est.1c02744

Notes

The authors declare no competing financial interest.

■ ACKNOWLEDGMENTS

This work was funded by the National Natural Science Foundation of China (41829701, 41921004, 42007307, and 41430754) and China Postdoctoral Science Foundation (2020M673300). The data used in this study are tabulated in Supporting Information.

■ REFERENCES

(1) Lindberg, S.; Bullock, R.; Ebinghaus, R.; Engstrom, D.; Feng, X.; Fitzgerald, W.; Pirrone, N.; Prestbo, E.; Seigneur, C. A synthesis of progress and uncertainties in attributing the sources of mercury in deposition. *Ambio* **2007**, *36*, 19−33.

(2) AMAP/UNEP. *AMAP/UNEP Geospatially Distributed Mercury Emissions Dataset 2010v1*, 2013.

(3) Agnan, Y.; Le Dantec, T.; Moore, C. W.; Edwards, G. C.; Obrist, D. New Constraints on Terrestrial Surface-Atmosphere Fluxes of Gaseous Elemental Mercury Using a Global Database. *Environ. Sci. Technol.* **2016**, *50*, 507−524.

(4) Zhou, J.; Obrist, D.; Dastoor, A.; Jiskra, M.; Ryjkov, A. Vegetation uptake of mercury and impacts on global cycling. *Nat. Rev. Earth Environ.* **2021**, *2*, 269−284.

(5) Bash, J. O.; Miller, D. R.; Meyer, T. H.; Bresnahan, P. A. Northeast United States and Southeast Canada natural mercury emissions estimated with a surface emission model. *Atmos. Environ.* **2004**, *38*, 5683−5692.

(6) Zhang, H.; Lindberg, S. E.; Marsik, F. J.; Keeler, G. J. Mercury air/surface exchange kinetics of background soils of the Tahquamenon River watershed in the Michigan Upper Peninsula. *Water, Air, Soil Pollut.* **2001**, *126*, 151−169.

(7) Wang, X.; Lin, C.-J.; Feng, X. Sensitivity analysis of an updated bidirectional air-surface exchange model for elemental mercury vapor. *Atmos. Chem. Phys.* **2014**, *14*, 6273−6287.

(8) Zhou, J.; Wang, Z.; Zhang, X.; Driscoll, C. T. Measurement of the Vertical Distribution of Gaseous Elemental Mercury Concentration in Soil Pore Air of Subtropical and Temperate Forests. *Environ. Sci. Technol.* **2021**, *55*, 2132−2142.

(9) Obrist, D.; Pokharel, A. K.; Moore, C. Vertical Profile Measurements of Soil Air Suggest Immobilization of Gaseous Elemental Mercury in Mineral Soil. *Environ. Sci. Technol.* **2014**, *48*, 2242−2252.

(10) Sigler, J. M.; Lee, X. Gaseous mercury in background forest soil in the northeastern United States. *J. Geophys. Res.: Biogeosci.* **2006**, *111*, G02007.

(11) Zhu, W.; Lin, C.-J.; Wang, X.; Sommar, J.; Fu, X.; Feng, X. Global observations and modeling of atmosphere-surface exchange of elemental mercury: a critical review. *Atmos. Chem. Phys.* **2016**, *16*, 4451−4480.

(12) Obrist, D.; Roy, E. M.; Harrison, J. L.; Kwong, C. F.; Munger, J. W.; Moosmüller, H.; Romero, C. D.; Sun, S.; Zhou, J.; Commane, R. Previously unaccounted atmospheric mercury deposition in a midlatitude deciduous forest. *Proc. Natl. Acad. Sci.* **2021**, *118*, No. e2105477118.

(13) Yu, Q.; Luo, Y.; Xu, G.; Wu, Q.; Wang, S.; Hao, J.; Duan, L. Subtropical Forests Act as Mercury Sinks but as Net Sources of Gaseous Elemental Mercury in South China. *Environ. Sci. Technol.* **2020**, *54*, 2772−2779.

(14) Wang, X.; Bao, Z.; Lin, C.-J.; Yuan, W.; Feng, X. Assessment of Global Mercury Deposition through Litterfall. *Environ. Sci. Technol.* **2016**, *50*, 8548−8557.

(15) Zheng, W.; Obrist, D.; Weis, D.; Bergquist, B. A. Mercury isotope compositions across North American forests. *Global Biogeochem. Cycles* **2016**, *30*, 1475−1492.

(16) Wang, X.; Yuan, W.; Lin, C.-J.; Zhang, L.; Zhang, H.; Feng, X. Climate and Vegetation As Primary Drivers for Global Mercury Storage in Surface Soil. *Environ. Sci. Technol.* **2019**, *53*, 10665−10675.

(17) Yuan, W.; Wang, X.; Lin, C.-J.; Wu, C.; Zhang, L.; Wang, B.; Sommar, J.; Lu, Z.; Feng, X. Stable Mercury Isotope Transition during Postdepositional Decomposition of Biomass in a Forest Ecosystem over Five Centuries. *Environ. Sci. Technol.* **2020**, *54*, 8739−8749.

(18) Jiskra, M.; Wiederhold, J. G.; Skyllberg, U.; Kronberg, R.-M.; Hajdas, I.; Kretzschmar, R. Mercury Deposition and Re-emission Pathways in Boreal Forest Soils Investigated with Hg Isotope Signatures. *Environ. Sci. Technol.* **2015**, *49*, 7188−7196.

(19) Demers, J. D.; Blum, J. D.; Zak, D. R. Mercury isotopes in a forested ecosystem: Implications for air-surface exchange dynamics and the global mercury cycle. *Global Biogeochem. Cycles* **2013**, *27*, 222−238.

(20) Li, K.; Lin, C.-J.; Yuan, W.; Sun, G.; Fu, X.; Feng, X. An improved method for recovering and preconcentrating mercury in natural water samples for stable isotope analysis. *J. Anal. At. Spectrom.* **2019**, *34*, 2303−2313.

(21) Wang, X.; Yuan, W.; Lin, C.-J.; Luo, J.; Wang, F.; Feng, X.; Fu, X.; Liu, C. Underestimated Sink of Atmospheric Mercury in a Deglaciated Forest Chronosequence. *Environ. Sci. Technol.* **2020**, *54*, 8083−8093.

(22) Wang, X.; Luo, J.; Yuan, W.; Lin, C.-J.; Wang, F.; Liu, C.; Wang, G.; Feng, X. Global warming accelerates uptake of atmospheric mercury in regions experiencing glacier retreat. *Proc. Natl. Acad. Sci.* **2020**, *117*, 2049−2055.

(23) Yu, B.; Fu, X.; Yin, R.; Zhang, H.; Wang, X.; Lin, C.-J.; Wu, C.; Zhang, Y.; He, N.; Fu, P.; Wang, Z.; Shang, L.; Sommar, J.; Sonke, J. E.; Maurice, L.; Guinot, B.; Feng, X. Isotopic Composition of Atmospheric Mercury in China: New Evidence for Sources and Transformation Processes in Air and in Vegetation. *Environ. Sci. Technol.* **2016**, *50*, 9262−9269.

(24) Yuan, W.; Sommar, J.; Lin, C.-J.; Wang, X.; Li, K.; Liu, Y.; Zhang, H.; Lu, Z.; Wu, C.; Feng, X. Stable Isotope Evidence Shows Re-emission of Elemental Mercury Vapor Occurring after Reductive Loss from Foliage. *Environ. Sci. Technol.* **2019**, *53*, 651−660.

(25) Fu, X.; Zhang, H.; Liu, C.; Zhang, H.; Lin, C.-J.; Feng, X. Significant Seasonal Variations in Isotopic Composition of Atmospheric Total Gaseous Mercury at Forest Sites in China Caused by Vegetation and Mercury Sources. *Environ. Sci. Technol.* **2019**, *53*, 13748−13756.

(26) Fu, X.; Zhu, W.; Zhang, H.; Sommar, J.; Yu, B.; Yang, X.; Wang, X.; Lin, C.-J.; Feng, X. Depletion of atmospheric gaseous elemental mercury by plant uptake at Mt. Changbai, Northeast China. *Atmos. Chem. Phys.* **2016**, *16*, 12861−12873.

(27) Kurz, A. Y.; Blum, J. D.; Gratz, L. E.; Jaffe, D. A. Contrasting Controls on the Diel Isotopic Variation of Hg0 at Two High Elevation Sites in the Western United States. *Environ. Sci. Technol.* **2020**, *54*, 10502−10513.

(28) Wang, X.; Zhang, H.; Lin, C. J.; Fu, X.; Zhang, Y.; Feng, X. Transboundary transport and deposition of Hg emission from springtime biomass burning in the Indo-China Peninsula. *J. Geophys. Res.: Atmos.* **2015**, *120*, 9758−9771.

(29) Zhang, H.; Fu, X.; Lin, C.-J.; Shang, L.; Zhang, Y.; Feng, X.; Lin, C. Monsoon-facilitated characteristics and transport of atmospheric mercury at a high-altitude background site in southwestern China. *Atmos. Chem. Phys.* **2016**, *16*, 13131−13148.

(30) Obrist, D.; Agnan, Y.; Jiskra, M.; Olson, C. L.; Colegrove, D. P.; Hueber, J.; Moore, C. W.; Sonke, J. E.; Helmig, D. Tundra uptake of atmospheric elemental mercury drives Arctic mercury pollution. *Nature* **2017**, *547*, 201−204.

(31) Blum, J. D.; Johnson, M. W. Recent Developments in Mercury Stable Isotope Analysis. *Rev. Mineral. Geochem.* **2017**, *82*, 733−757.

(32) Blum, J. D.; Sherman, L. S.; Johnson, M. W. Mercury Isotopes in Earth and Environmental Sciences. *Annu. Rev. Earth Planet Sci.* **2014**, *42*, 249−269.

(33) Kritee, K.; Blum, J. D.; Barkay, T. Mercury Stable Isotope Fractionation during Reduction of Hg(II) by Different Microbial Pathways. *Environ. Sci. Technol.* **2008**, *42*, 9171−9177.

(34) Kritee, K.; Blum, J. D.; Johnson, M. W.; Bergquist, B. A.; Barkay, T. Mercury stable isotope fractionation during reduction of Hg(II) to Hg(0) by mercury resistant microorganisms. *Environ. Sci. Technol.* **2007**, *41*, 1889−1895.

(35) Jiskra, M.; Sonke, J. E.; Agnan, Y.; Helmig, D.; Obrist, D. Insights from mercury stable isotopes on terrestrial-atmosphere exchange of Hg(0) in the Arctic tundra. *Biogeosciences* **2019**, *16*, 4051−4064.

(36) Zheng, W.; Demers, J. D.; Lu, X.; Bergquist, B. A.; Anbar, A. D.; Blum, J. D.; Gu, B. Mercury Stable Isotope Fractionation during Abiotic Dark Oxidation in the Presence of Thiols and Natural Organic Matter. *Environ. Sci. Technol.* **2019**, *53*, 1853−1862.

(37) Zheng, W.; Hintelmann, H. Nuclear Field Shift Effect in Isotope Fractionation of Mercury during Abiotic Reduction in the Absence of Light. *J. Phys. Chem. A* **2010**, *114*, 4238−4245.

(38) Zheng, W.; Hintelmann, H. Isotope Fractionation of Mercury during Its Photochemical Reduction by Low-Molecular-Weight Organic Compounds. *J. Phys. Chem. A* **2010**, *114*, 4246−4253.

(39) Zheng, W.; Hintelmann, H. Mercury isotope fractionation during photoreduction in natural water is controlled by its Hg/DOC ratio. *Geochim. Cosmochim. Acta* **2009**, *73*, 6704−6715.

(40) Bergquist, B. A.; Blum, J. D. Mass-dependent and -independent fractionation of Hg isotopes by photoreduction in aquatic systems. *Science* **2007**, *318*, 417−420.

(41) Fu, X.; Zhang, H.; Feng, X.; Tan, Q.; Ming, L.; Liu, C.; Zhang, L. Domestic and Transboundary Sources of Atmospheric Particulate Bound Mercury in Remote Areas of China: Evidence from Mercury Isotopes. *Environ. Sci. Technol.* **2019**, *53*, 1947−1957.

(42) Yuan, W.; Wang, X.; Lin, C.-J.; Sommar, J.; Lu, Z.; Feng, X. Process factors driving dynamic exchange of elemental mercury vapor over soil in broadleaf forest ecosystems. *Atmos. Environ.* **2019**, *219*, 117047.

(43) Wang, X.; Yuan, W.; Lu, Z.; Lin, C. J.; Yin, R.; Li, F.; Feng, X. Effects of Precipitation on Mercury Accumulation on Subtropical Montane Forest Floor: Implications on Climate Forcing. *J. Geophys. Res.: Biogeosci.* **2019**, *124*, 959−972.

(44) Wen, H.-D.; Lin, L.-X.; Yang, J.; Hu, Y.-H.; Cao, M.; Liu, Y.-H.; Lu, Z.-Y.; Xie, Y.-N. Species composition and community structure of a 20 hm^2 plot of mid-mountain moist evergreen broad-leaved forest on the Mts. Ailaoshan, Yunnan Province, China. *Chin. J. Plant Ecol.* **2018**, *42*, 419−429.

(45) Sprovieri, F.; Pirrone, N.; Bencardino, M.; D'Amore, F.; Carbone, F.; Cinnirella, S.; Mannarino, V.; Landis, M.; Ebinghaus, R.; Weigelt, A.; Brunke, E.-G.; Labuschagne, C.; Martin, L.; Munthe, J.; Wängberg, I.; Artaxo, P.; Morais, F.; Barbosa, H. d. M. J.; Brito, J.; Cairns, W.; Barbante, C.; Diéguez, M. d. C.; Garcia, P. E.; Dommergue, A.; Angot, H.; Magand, O.; Skov, H.; Horvat, M.; Kotnik, J.; Read, K. A.; Neves, L. M.; Gawlik, B. M.; Sena, F.; Mashyanov, N.; Obolkin, V.; Wip, D.; Feng, X. B.; Zhang, H.; Fu, X.; Ramachandran, R.; Cossa, D.; Knoery, J.; Marusczak, N.; Nerentorp, M.; Norstrom, C. Atmospheric mercury concentrations observed at ground-based monitoring sites globally distributed in the framework of the GMOS network. *Atmos. Chem. Phys.* **2016**, *16*, 11915−11935.

(46) Fu, X.; Heimbürger, L.-E.; Sonke, J. E. Collection of atmospheric gaseous mercury for stable isotope analysis using iodine- and chlorine-impregnated activated carbon traps. *J. Anal. At. Spectrom.* **2014**, *29*, 841−852.

(47) Sommar, J.; Osterwalder, S.; Zhu, W. Recent advances in understanding and measurement of Hg in the environment: Surface-atmosphere exchange of gaseous elemental mercury (Hg0). *Sci. Total Environ.* **2020**, *721*, 137648.

https://doi.org/10.1021/acs.est.1c02744
Environ. Sci. Technol. XXXX, XXX, XXX−XXX

(48) Lin, C.-J.; Zhu, W.; Li, X.; Feng, X.; Sommar, J.; Shang, L. Novel Dynamic Flux Chamber for Measuring Air-Surface Exchange of Hgo from Soils. *Environ. Sci. Technol.* **2012**, *46*, 8910−8920.

(49) Sun, R.; Enrico, M.; Heimbürger, L.-E.; Scott, C.; Sonke, J. E. A double-stage tube furnace-acid-trapping protocol for the pre-concentration of mercury from solid samples for isotopic analysis. *Anal. Bioanal. Chem.* **2013**, *405*, 6771−6781.

(50) US—EPA. *Method 1631, Revision E: Mercury in Water by Oxidation, Purge and Trap, and Cold Vapor Atomic Fluorescence Spectrometry*. 2002.

(51) Yin, R.-S.; Feng, X.-B.; Foucher, D.; Shi, W.-F.; Zhao, Z.-Q.; Wang, J. High Precision Determination of Mercury Isotope Ratios Using Online Mercury Vapor Generation System Coupled with Multicollector Inductively Coupled Plasma-Mass Spectrometer. *Chin. J. Anal. Chem.* **2010**, *38*, 929−934.

(52) Wang, X.; Luo, J.; Yin, R.; Yuan, W.; Lin, C.-J.; Sommar, J.; Feng, X.; Wang, H.; Lin, C. Using Mercury Isotopes To Understand Mercury Accumulation in the Montane Forest Floor of the Eastern Tibetan Plateau. *Environ. Sci. Technol.* **2017**, *51*, 801−809.

(53) Koster van Groos, P. G.; Esser, B. K.; Williams, R. W.; Hunt, J. R. Isotope Effect of Mercury Diffusion in Air. *Environ. Sci. Technol.* **2014**, *48*, 227−233.

(54) Nacht, D. M.; Gustin, M. S. Mercury emissions from background and altered geologic units throughout Nevada. *Water, Air, Soil Pollut.* **2004**, *151*, 179−193.

(55) Zhou, J.; Wang, Z.; Zhang, X.; Sun, T. Investigation of factors affecting mercury emission from subtropical forest soil: A field controlled study in southwestern China. *J. Geochem. Explor.* **2017**, *176*, 128−135.

(56) Gustin, M. S.; Stamenkovic, J. Effect of watering and soil moisture on mercury emissions from soils. *Biogeochemistry* **2005**, *76*, 215−232.

(57) Kuss, J.; Holzmann, J.; Ludwig, R. An Elemental Mercury Diffusion Coefficient for Natural Waters Determined by Molecular Dynamics Simulation. *Environ. Sci. Technol.* **2009**, *43*, 3183−3186.

(58) Tsipis, A. C. Interaction of Elemental Mercury with a Diverse Series of π-Organic Substrates Probed by Computational Methods: Is Mercury Fixation Possible? *ACS Earth Space Chem.* **2018**, *2*, 451−461.

(59) Wang, Y.; Li, Y.; Liu, G.; Wang, D.; Jiang, G.; Cai, Y. Elemental Mercury in Natural Waters: Occurrence and Determination of Particulate Hg(0). *Environ. Sci. Technol.* **2015**, *49*, 9742−9749.

(60) Landa, E. R. The retention of metallic mercury vapor by soils. *Geochim. Cosmochim. Acta* **1978**, *42*, 1407−1411.

(61) Wang, X.; Lin, C.-J.; Yuan, W.; Sommar, J.; Zhu, W.; Feng, X. Emission-dominated gas exchange of elemental mercury vapor over natural surfaces in China. *Atmos. Chem. Phys.* **2016**, *16*, 11125−11143.

(62) Kuiken, T.; Gustin, M.; Zhang, H.; Lindberg, S.; Sedinger, B. Mercury emission from terrestrial background surfaces in the eastern USA. II: Air/surface exchange of mercury within forests from South Carolina to New England. *Appl. Geochem.* **2008**, *23*, 356−368.

(63) Briggs, C.; Gustin, M. S. Building upon the Conceptual Model for Soil Mercury Flux: Evidence of a Link Between Moisture Evaporation and Hg Evasion. *Water, Air, Soil Pollut.* **2013**, *224*, 1744.

(64) Guédron, S.; Amouroux, D.; Tessier, E.; Grimaldi, C.; Barre, J.; Berail, S.; Perrot, V.; Grimaldi, M. Mercury Isotopic Fractionation during Pedogenesis in a Tropical Forest Soil Catena (French Guiana): Deciphering the Impact of Historical Gold Mining. *Environ. Sci. Technol.* **2018**, *52*, 11573−11582.

(65) Moore, C. W.; Castro, M. S. Investigation of factors affecting gaseous mercury concentrations in soils. *Sci. Total Environ.* **2012**, *419*, 136−143.

(66) Wang, X.; Lin, C.-J.; Lu, Z.; Zhang, H.; Zhang, Y.; Feng, X. Enhanced accumulation and storage of mercury on subtropical evergreen forest floor: Implications on mercury budget in global forest ecosystems. *J. Geophys. Res.: Biogeosci.* **2016**, *121*, 2096−2109.

(67) Zhou, J.; Feng, X.; Liu, H.; Zhang, H.; Fu, X.; Bao, Z.; Wang, X.; Zhang, Y. Examination of total mercury inputs by precipitation and litterfall in a remote upland forest of Southwestern China. *Atmos. Environ.* **2013**, *81*, 364−372.

(68) Jiskra, M.; Wiederhold, J. G.; Bourdon, B.; Kretzschmar, R. Solution Speciation Controls Mercury Isotope Fractionation of Hg(II) Sorption to Goethite. *Environ. Sci. Technol.* **2012**, *46*, 6654−6662.

(69) Zheng, W.; Liang, L.; Gu, B. Mercury Reduction and Oxidation by Reduced Natural Organic Matter in Anoxic Environments. *Environ. Sci. Technol.* **2012**, *46*, 292−299.

(70) Zheng, W.; Lin, H.; Mann, B. F.; Liang, L.; Gu, B. Oxidation of Dissolved Elemental Mercury by Thiol Compounds under Anoxic Conditions. *Environ. Sci. Technol.* **2013**, *47*, 12827−12834.

(71) Scholtz, M. T.; Van Heyst, B. J.; Schroeder, W. H. Modelling of mercury emissions from background soils. *Sci. Total Environ.* **2003**, *304*, 185−207.

(72) Wiederhold, J. G.; Cramer, C. J.; Daniel, K.; Infante, I.; Bourdon, B.; Kretzschmar, R. Equilibrium Mercury Isotope Fractionation between Dissolved Hg(II) Species and Thiol-Bound Hg. *Environ. Sci. Technol.* **2010**, *44*, 4191−4197.

(73) Amos, H. M.; Jacob, D. J.; Streets, D. G.; Sunderland, E. M. Legacy impacts of all-time anthropogenic emissions on the global mercury cycle. *Global Biogeochem. Cycles* **2013**, *27*, 410−421.

(74) Corbitt, E. S.; Jacob, D. J.; Holmes, C. D.; Streets, D. G.; Sunderland, E. M. Global Source-Receptor Relationships for Mercury Deposition Under Present-Day and 2050 Emissions Scenarios. *Environ. Sci. Technol.* **2011**, *45*, 10477−10484.

(75) Selin, N. E.; Jacob, D. J.; Yantosca, R. M.; Strode, S.; Jaegle, L.; Sunderland, E. M. Global 3-D land-ocean-atmosphere model for mercury: Present-day versus preindustrial cycles and anthropogenic enrichment factors for deposition. *Global Biogeochem. Cycles* **2008**, *22*, GB2011.

(76) Smith-Downey, N. V.; Sunderland, E. M.; Jacob, D. J. Anthropogenic impacts on global storage and emissions of mercury from terrestrial soils: Insights from a new global model. *J. Geophys. Res.: Biogeosci.* **2010**, *115*, G03008.

(77) Sonke, J. E.; Blum, J. D. Advances in mercury stable isotope biogeochemistry. *Chem. Geol.* **2013**, *336*, 1−4.

(78) Tsui, M. T.-K.; Blum, J. D.; Kwon, S. Y. Review of stable mercury isotopes in ecology and biogeochemistry. *Sci. Total Environ.* **2020**, *716*, 135386.

(79) Kwon, S. Y.; Blum, J. D.; Yin, R.; Tsui, M. T.-K.; Yang, Y. H.; Choi, J. W. Mercury stable isotopes for monitoring the effectiveness of the Minamata Convention on Mercury. *Earth-Sci. Rev.* **2020**, *203*, 103111.

(80) Cantrell, C. A. Technical Note: Review of methods for linear least-squares fitting of data and application to atmospheric chemistry problems. *Atmos. Chem. Phys.* **2008**, *8*, 5477−5487.